ResearchGate

See discussions, stats, and author profiles for this publication at: https://www.researchgate.net/publication/51543344

In Situ Curing of Sliding SU-8 Droplet over a Microcontact Printed Pattern for Tunable Fabrication of a Polydimethylsiloxane Nanoslit

ARTICLE *in* ANALYTICAL CHEMISTRY · AUGUST 2011

Impact Factor: 5.64 · DOI: 10.1021/ac200859b · Source: PubMed

CITATION
1

READS
27

7 AUTHORS, INCLUDING:

Chang-Beom Kim
Electronics and Telecommunications Resear…
20 PUBLICATIONS **282** CITATIONS
SEE PROFILE

Jaehun Chung
ASML
13 PUBLICATIONS **70** CITATIONS
SEE PROFILE

jeong hoon Lee
Kwangwoon University
184 PUBLICATIONS **2,093** CITATIONS
SEE PROFILE

Sang-Hoon Lee
Korea University
405 PUBLICATIONS **5,461** CITATIONS
SEE PROFILE

Available from: Sang-Hoon Lee
Retrieved on: 29 January 2016

analytical chemistry

TECHNICAL NOTE

pubs.acs.org/ac

In Situ Curing of Sliding SU-8 Droplet over a Microcontact Printed Pattern for Tunable Fabrication of a Polydimethylsiloxane Nanoslit

Chang-Beom Kim,[†,⊥] Honggu Chun,[†] JaeHun Chung,[‡] Kwang Ho Lee,[§] Jeong Hoon Lee,[∥] Ki-Bong Song,[⊥] and Sang-Hoon Lee*[,†]

[†]Department of Biomedical Engineering, Korea University, Seoul, 136-703, Korea

[‡]Department of Mechanical Engineering, Korea University, Seoul, 136-713, Korea

[§]Department of Advanced Materials Science and Engineering, Kangwon National University, Chuncheon, 200-701, Korea

[∥]Department of Electrical Engineering, Kwangwoon University, Seoul, 139-701, Korea

[⊥]Creative and Challenging Research Division, Electronics and Telecommunications Research Institute, Daejeon, 305-700, Korea

Supporting Information

ABSTRACT: A tunable process for polydimethylsiloxane (PDMS) nanoslit fabrication is developed for nanofluidic applications. A microcontact printing (μCP) of a laterally spreading self-assembled hexadecanethiol (HDT) layer, combined with in situ curing of a sliding SU-8 droplet, enables precise and independent tuning of a nanoslit-mold width and height using a single μCP master mold. The SU-8 nanoslit-mold is replicated using a hard−soft composite PDMS to prevent channel collapse at low (<0.2) aspect ratio (height over width). The fluidic characteristics as well as dimensions of nanoslits fabricated with various conditions are analyzed using a fluorescein sample and AFM images. Finally, concentration polarization-based sample preconcentration is successfully demonstrated at the nanoslit boundary where an electric double-layer is overlapped.

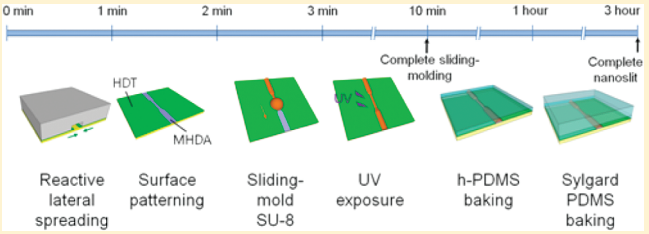

Nanoscale fluidic structures have attracted great attention due to their potential applications in areas such as ion transport,[1−4] DNA analysis,[5,6] immune-biosensing,[7] and fuel cells.[8,9] To date, most nanochannel fabrication techniques have been principally based on e-beam lithography[10,11] or nanoimprint lithography.[12,13] Although these methods have greatly contributed to the fabrication of well-defined nanochannels, they require complicated, time-consuming, and labor-dependent processes and high-end devices. In addition, the mass production of nanochannel systems is challenging, and channel materials have been limited to glass and silicon wafers. Over the last 10 years, polydimethylsiloxane (PDMS) has been extensively used in chemical and biomedical fields because PDMS is inert to biological objects and has a high water and gas permeability.[14,15] Recently, several researchers have used PDMS to form nanofluidic channels,[16−18] and the combination of nanochannels networked with microfluidic technologies extends the applications of nanochannels.[19−22] However, the nanochannel-mold for the PDMS replication required complicated fabrication processes and its dimensions were not tunable. Moreover, the fabrication of PDMS nanochannels with low (<0.2) aspect ratio (height over width) has posed tremendous challenges due to collapse of the soft PDMS and complex fabrication process.

In this paper, we propose a simple, fast, and cost-effective fabrication method for a low aspect ratio PDMS nanoslit with independently tunable width and height using a single master mold. The fabrication process consists of three steps: (1) the patterning of self-assembled hydrophobic/hydrophilic monolayers on a gold substrate using microcontact printing (μCP);[23−25] (2) the fabrication of nanoslit-molds by sliding SU-8 droplet in situ curing on the hydrophilic-patterned surface which is tilted at an angle; and (3) the replication of the nanoslit structure from SU-8 molds using composite layers of hard and soft PDMS that prevent the channel collapse.[26−28] The major feature of the method is that the SU-8 nanoslit molds width and height are independently tunable with a single master mold by simply changing contact printing time (channel width), sliding speed of the SU-8 droplet, and SU-8 viscosity (channel height), respectively. Moreover, obtaining a rounded mold rather than square cross-sectional shapes is also a difference from other methods. The arch-shaped cross-section of a PDMS nanoslit is advantageous to sustain the structure of low aspect ratio without collapse. The fabricated noncollapsible PDMS nanoslit was then bonded to glass microchannels to form a complete fluidic network. The fluidic characteristic of the nanoslit was monitored using an anion fluorescent dye, fluorescein, at various buffer concentrations. The nanoslits showed cation perm-selectivity at lower buffer concentrations due to electric double-layer (EDL)

Received: April 5, 2011
Accepted: August 3, 2011
Published: August 03, 2011

ACS Publications © 2011 American Chemical Society

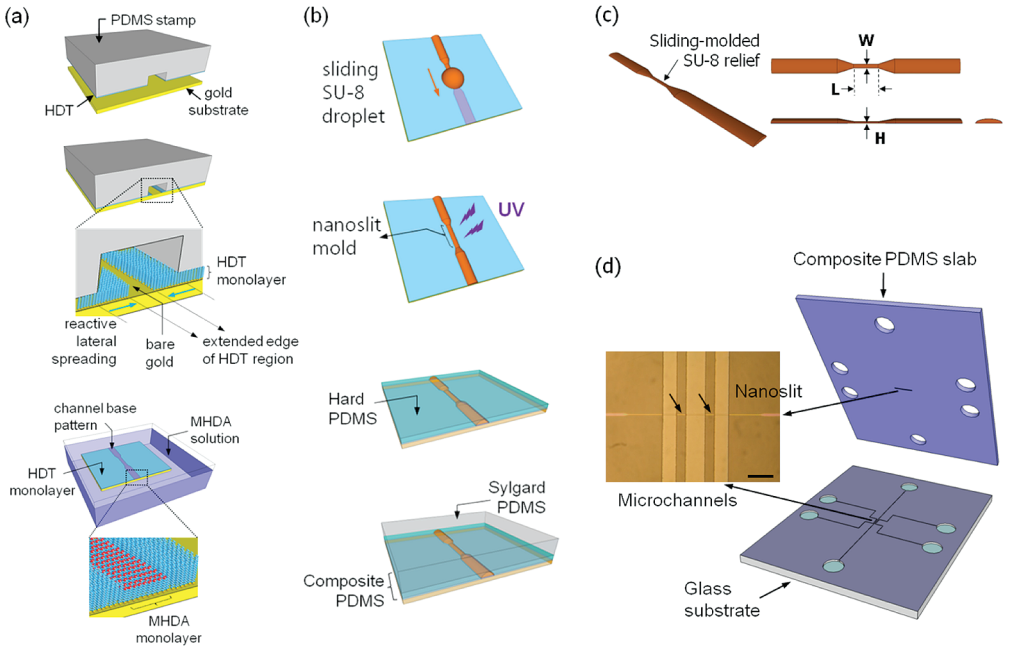

Figure 1. Rapid prototyping processes for the fabrication of the nanoslit. (a) μCP process for hydrophilic/hydrophobic alkanethiol surface patterning on gold substrate. The nanoslit width is reduced by increasing reactive lateral spreading of HDT into bare gold region. (b) Self-organization of SU-8 on MHDA monolayer during sliding of SU-8 droplet on the tilted patterned substrate. PDMS replication from SU-8 mold using composite PDMS to generate a noncollapsible nanoslit device with low height. (c) Schematics and dimension of the nanoslit mold (height, 41.4−76.8 nm for SU-8 2, 105.3 to 179.2 nm for 1:1 mixture; width, 2.12−3.24 μm for both SU-8 cases). (d) Schematics of nanoslit device networked with microchannels (inset) 500 μm long nanoslit perpendicularly traversing the three microchannels. The scale bar represents 100 μm.

overlap conditions. The nanoslit height could be estimated from the maximum buffer concentration, demonstrating the cation perm-selectivity, which showed good agreement with the SU-8 mold height measured by AFM. Nanoslit ion perm-selectivity extends their applications to biomedical sample manipulations, including electropreconcentration. Finally, we successfully demonstrated electropreconcentration using PDMS nanoslits.

MATERIALS AND METHODS

Nanoslit Fabrication. Figure 1 shows an overall schematic diagram describing the rapid prototyping processes for the noncollapsible PDMS nanoslit. Figure 1a illustrates the μCP process for surface functionalization by micropatterning hydrophobic/hydrophilic alkanethiol monolayers on a gold substrate to form heterogeneous wetting/dewetting regions. A gold layer (thickness of 600 Å, evaporation rate of 1.0 Å/s) was deposited onto a titanium-primed (thickness of 150 Å, evaporation rate of 0.5 Å/s) silicon wafer at a pressure of 6×10^{-6} Torr. A PDMS (Sylgard 184, Dow Corning Corporation, MI) stamp was replicated from a photolithographically produced SU-8 (Microchem, MA) master mold and then was used as a surface patterning tool, producing uniform contact on the gold substrate. The PDMS stamp for the nanoslit patterning was 3.6 μm × 6 μm × 500 μm in width, depth, and length, respectively.

The PDMS stamp was inked with a hydrophobic thiol solution, 2 mM hexadecanethiol (HDT, Sigma-Aldrich, MO) in anhydrous ethanol, by immersing the surface of the stamp in the thiol solution for 30 s prior to contact printing. The stamp was gently dried by exposing to a stream of nitrogen gas so that the HDT residues trapped in the intaglio of the stamp did not disturb the channel shape patterns. The stamp was then contacted over the gold substrate and slight pressure was applied, allowing the HDT ink to transfer onto the gold surface. During the contact printing process, the edge of the HDT region under the contact area of the stamp was extended into the noncontact bare gold area by the reactive lateral spreading of HDT molecules,[29] and this spreading reduced the width of the nanoslit pattern (bare gold area).[30,31] The final width of the channel pattern could be precisely controlled by adjusting the stamp contact time because the HDT lateral spreading is slow and uniform. The HDT patterned gold substrate was thereafter exposed to a hydrophilic thiol solution, 1 mM mercaptohexadecanoic acid (MHDA, Sigma-Aldrich, MO), for 10 s to convert the nonpatterned regions into hydrophilic surfaces.[32] Then, the excessive thiols were removed using ethanol.

The SU-8 mold for the nanoslit was then self-organized on the HDT/MHDA patterned substrate (Figure 1b). An SU-8 droplet (~5 μL) was dropped onto the HDT/MHDA patterned surface. We tilted the substrate to allow the SU-8 droplet to slide downward along the MHDA patterned area (channel base shape). Then, a liquid SU-8 nanostructure (in height) was self-organized onto the wet surface and polymerized by UV irradiation for 5 min. The mold height could be controlled as a function of the substrate tilting angle and the SU-8 viscosity. Figure 1c represents the schematic features of the SU-8 mold with nanodimensional height (H) and microdimensional length (L) and width (W).

For the fabrication of the noncollapsible PDMS nanoslit of low aspect ratio via replication of the SU-8 mold, the mechanical characteristics of the elastomeric elements are critically important. A previous study suggested that a composite of two PDMS layers (thin stiff layer and thick soft layer) enables the fabrication of a stamp whose width is less than 100 nm without collapse or

dx.doi.org/10.1021/ac200859b |*Anal. Chem.* 2011, 83, 7221–7226

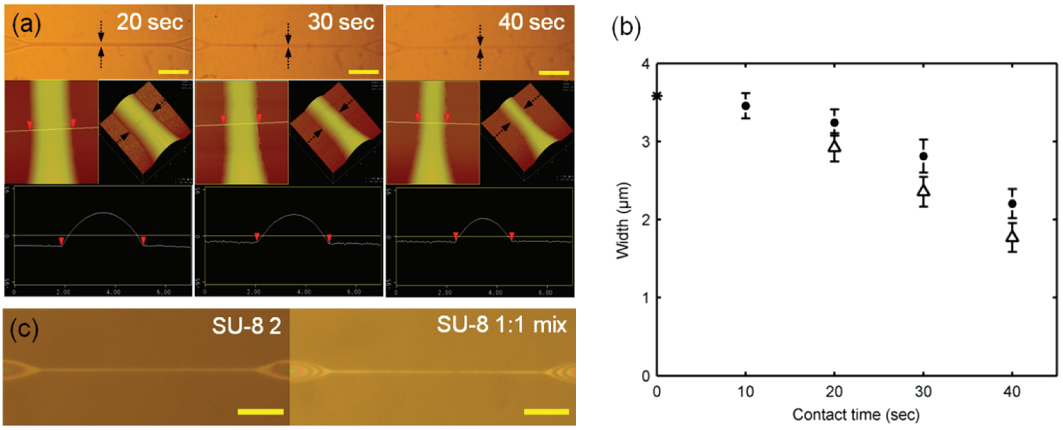

Figure 2. (a) (upper) Optical images of SU-8 molds by adjusting the stamping contact time ranged from 20 to 40 s (tilting angle 20°). Scale bar represents 20 μm. (lower) the corresponding 2D/3D AFM images of the SU-8 molds and the cross-sectional profiles revealing the reduction of width. (b) Variations of the mold width (●, $n = 6$) as a function of contact printing time. Dimensions were measured by AFM. The replicated PDMS nanoslit width (△, $n = 6$) was slightly smaller than those of the molds due to PDMS shrink after thermal curing. The nanoslit for 10 s could not be formed due to very small height of the mold. ∗ represents the width of the engraved pattern on the PDMS stamp. (c) Formation of composite PDMS nanoslits replicated from the SU-8 mold (40 s contact time). Two viscous SU-8 solutions were used to fabricate the SU-8 molds: The thinner solution (SU-8 2) generated molds with a lower height (≈ 50 nm), while the thicker (1:1 mixture) generated molds with higher heights (>100 nm).

buckling.[26] In this study, we used a thin hard (h)-PDMS layer to prevent roof collapse of the nanoslit and then soft (s)-PDMS was layered over the thin h-PDMS layer to alleviate the brittleness or cracking of h-PDMS.[28,33] Briefly, the h-PDMS was prepared from a mixture of trimethylsiloxy-terminated vinylmethylsiloxane-dimethylsiloxane (3.4 g, VDT-731, Gelest, PA), Pt catalysts (20 μL, platinum divinyltetramethyldisiloxane, Gelest, PA), and modulator (0.1 g, cyclooctane, Sigma-Aldrich, MO). Methylhydrosiloxane-dimethylsiloxane (1.0 g, HMS-301, Gelest, PA) copolymer was added to the mixture and gently stirred to prevent bubble generation. Hexane (2 g, Sigma-Aldrich, MO) was then blended with the above mixture to decrease the flexibility of the h-PDMS. Hexane decreased the viscosity of the h-PDMS by reducing the chain length, which promoted the brittleness but reduced the flexibility of the prepolymer.[34,35] To support the increased brittleness of the h-PDMS, which was a critical cause of structural cracking across the surface of the nanoslit-engraved slab, a Sylgard PDMS layer was added to the h-PDMS layer. The h-PDMS solution was coated (30−40 μm) onto the SU-8 mold, followed by curing at 60 °C for 60 min. Then, a relatively thick (~2 mm) layer of Sylgard PDMS was cured onto the h-PDMS layer at 60 °C for 2 h. The cured composite PDMS slab with replicated nanoslit structure was carefully peeled off, and access inlet/outlet holes were drilled. Figure 1d shows the schematic of the fluidic channel network connecting the nanoslit to buffered oxide etched (BOE) microchannels (depth of 12 μm, width of 50 μm) on a glass substrate. A 500 μm long nanoslit was plasma-bonded across three glass microchannels which are separated by 40 μm. The nanoslit was successfully formed without collapse (see the Supporting Information, Figure S1) between microchannels, as indicated by the arrows in the optical microscopy inset image (Figure 1d).

Ion Preconcentration. The micro/nano preconcentration chip was composed of three microchannels with a nanoslit perpendicularly traversing them (Figure 1d). The sample channel (S) was filled with fluorescein (10 μM, Sigma-Aldrich, MO) in sodium phosphate dibasic buffer (100, 200, and 1000 μM, Sigma-Aldrich, MO) at pH 7.4, and the drain (D) and gate (G) channels were filled with the same concentration buffer. To electrokinetically drive a tangential flow inside the middle channel, a potential difference was applied between the middle (V_S, V_D) and the side microchannels (V_G). The applied voltages for each case (100, 200, and 1000 μM) were V_S =150 V and V_D = 80, 95, 140 V, respectively. The concentration plug was analyzed by fluorescence microscopy.

RESULTS AND DISCUSSION

SU-8 Nanoslit Mold Width and Height Tuning. We investigated the effects of the stamping contact time, tilting angle, and SU-8 viscosity on the channel width and height. Figure 2a shows AFM images of the SU-8 nanoslit molds with different stamping contact time ranging from 20 to 40 s. As shown, the channel surface is extremely smooth, desirable for potential biochemical applications. Two- and three-dimensional topographical descriptions of nanoslit molds are presented as a function of contact time. As predicted, the widths of the SU-8 nanoslit molds decreased as the stamping contact time increased, quantitatively plotted in Figure 2b: when the contact time changed from 20 to 40 s, the mean widths of the nanoslit molds decreased from 3.24 to 2.12 μm; the mean heights of the molds also decreased from 68.8 nm (aspect ratio = 0.021) to 51.1 nm (aspect ratio = 0.024). This phenomenon is based on the fact that longer contact times apparently permit the lateral growth of HDT molecules into the noncontact bare gold regions on which the SU-8 structure had been self-organized.

After the nanoslit mold width is tuned, the channel height is then controlled as follows. The tilting angle (or sliding speed) and viscosity of SU-8 are important factors for controlling the height of the SU-8 mold. For the control of nanoslit mold height, two types of SU-8 with different viscosity were used: SU-8 2 (for the shallow nanoslit) and the 1:1 (v/v) mixture of SU-8 2 and SU-8 25 (for the deeper nanoslit). Figure 2c shows the successful formation of the composite PDMS nanoslit replicated from both SU-8 molds.

Figure 3a shows the droplet sliding speeds for various tilting angles of the substrate for different SU-8 solutions. Droplets (~5 μL) of the SU-8 2 and the 1:1 mixture solution were

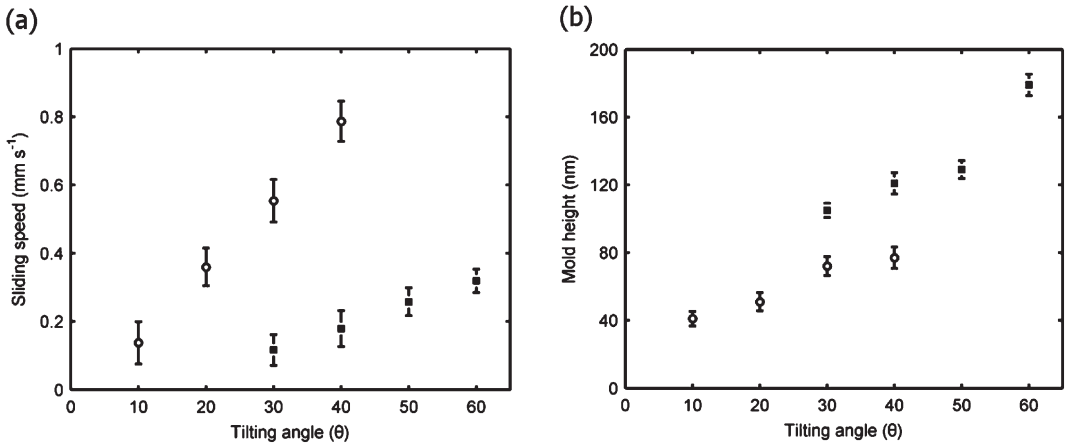

Figure 3. Height change of SU-8 molds by controlling the sliding speed of SU-8 droplets by changing the angle of the slanted substrate. Part a shows the droplet sliding speeds for various tilting angles of the substrate (○ for SU-8 2, ■ for 1:1 mixture, n = 3 each). The sliding speed linearly varied with the tilting angle. Part b shows the mold heights for the corresponding tilting angles of the substrate (○ for SU-8 2, ■ for 1:1 mixture, n = 5 each). The apparent differences in the mold height are expressed as a function of the tilting angle for the different SU-8 solutions (40 s contact time). Slow droplet speed reduced the mold height (see the Supporting Information, Figure S3) while fast droplet generated higher molds.

dropped at the top of the hydrophilic pattern. As predicted, the sliding speed of the droplet increased as the tilting angle became steeper, and the droplet sliding speed varied linearly. The tilting angles ranged from 10° to 40° for SU-8 2 and from 30° to 60° for the mixture. At the lower angle, the 1:1 mixture droplet crept much slower due to the viscosity. Interestingly, slow droplet speeds decreased the mold height, and fast droplet speeds increased the mold height (Figure 3b). This phenomenon is believed to be based on the viscoelastic properties of SU-8 during sliding. When the SU-8 droplet slowly passes over the hydrophilic region, the relatively larger volume of the sliding droplet recollects a substantial portion of trapped SU-8 from the hydrophilic surface. On the other hands, if the sliding speed increases, the droplet does not have sufficient time to recapture the trapped SU-8, and a larger SU-8 residue remains on the surface of the trapped SU-8 to produce a thicker sliding mold. Although the tilting angle and viscosity are critical in determining height, the width of nanoslit mold (1.7−2.1 μm) was not affected by either factor. This independent tuning of a SU-8 nanoslit mold width and height using a single master mold is the main difference from standard photolithography where multiple numbers of photomask and the spin-coat process are required for different mold dimensions. Obtaining rounded rather than square cross-sectional shapes is also a difference from other fabrication methods, which is believe to be advantageous to sustain the nanoslit structure.

Electropreconcentration. Here, we present an example of a practical application of the PDMS nanoslit to electropreconcentration of charged molecules. When the surface charge induced electric double-layers (EDL) of a nanoslit overlap (or near overlap, i.e., channel half height/EDL thickness <10), the nanoslit excludes co-ion (anion in this study). Then the nanoslits operate as counterion (cation in this study) permselective filters when an electric field is applied across the channel. The electric field produces a local field gradient near the micro/nanochannel junction, which results in concentration polarization and corresponding sample preconcentration.[19,36,37] Figure 4a describes the basic mechanism that regulates the electrokinetic trapping process during ion preconcentration using a nanoslit integrated with a microfluidic chip. When the G reservoirs are electrically floated, the sample solution is primarily governed by electroosmotic flow (EOF) along the middle channel, for $V_S > V_D$. Immediately upon application of V_G = 0 V, cations are permselectively extracted from the middle channel through the negatively charged nanoslit, while anions are evicted from the region near the micro−nano interface. Then an ion-depleted zone subsequently develops near the micro−nano interface. The electrophoretic (EP) velocity of the negatively charged fluorescein ions is augmented as a result of the considerably enhanced electric field in the ion-depleted region, whereas the EOF is stationary. Subsequently, the anions accumulate on the left-hand side of the ion-depletion area, and the concentrated plug is fairly stable where the EOF and EP find a balance.

Preconcentration experiments were performed using three different initial buffer concentrations (100, 200, and 1000 μM) with a constant sample concentration (10 μM). The applied voltages for each buffer concentration were V_S =150 V and V_D = 80, 95, 140 V, respectively. During operation, a balance between the anion repulsion from the ion-depletion area and the electroosmotic flow in the middle microchannel was maintained to preconcentrate the molecules, as described previously.[19,20,38−42]

By application of a potential difference, negatively charged fluorescein molecules concentrated at the left boundary of the ion-depleted region. Figure 4b shows fluorescence images showing the concentration of fluorescein at the micro−nanochannel interface, taken every 1 s over a 10 s period for a buffer concentration of 200 μM. As time passed, the fluorescence intensity increased linearly within 1 s, after which the concentrating effect leveled off. However, the preconcentrated sample plug size continued to increase so that the collected molecule number increased linearly (Figure 4c). Our results showed that stable electropreconcentration process was achieved with buffer concentrations up to 1 mM (see the Supporting Information, Figure S2). Considering that the electropreconcentration mechanism is observable with EDL overlap (or near overlap) conditions and the EDL thickness of the 1 mM phosphate buffer was 6 nm, these results demonstrate that the μCP and the composite PDMS nanoslits retained the nanothin channel structure. In addition, optical microscopy image analysis showed no sample leakage through the PDMS−glass bonding layer, implying that the ion

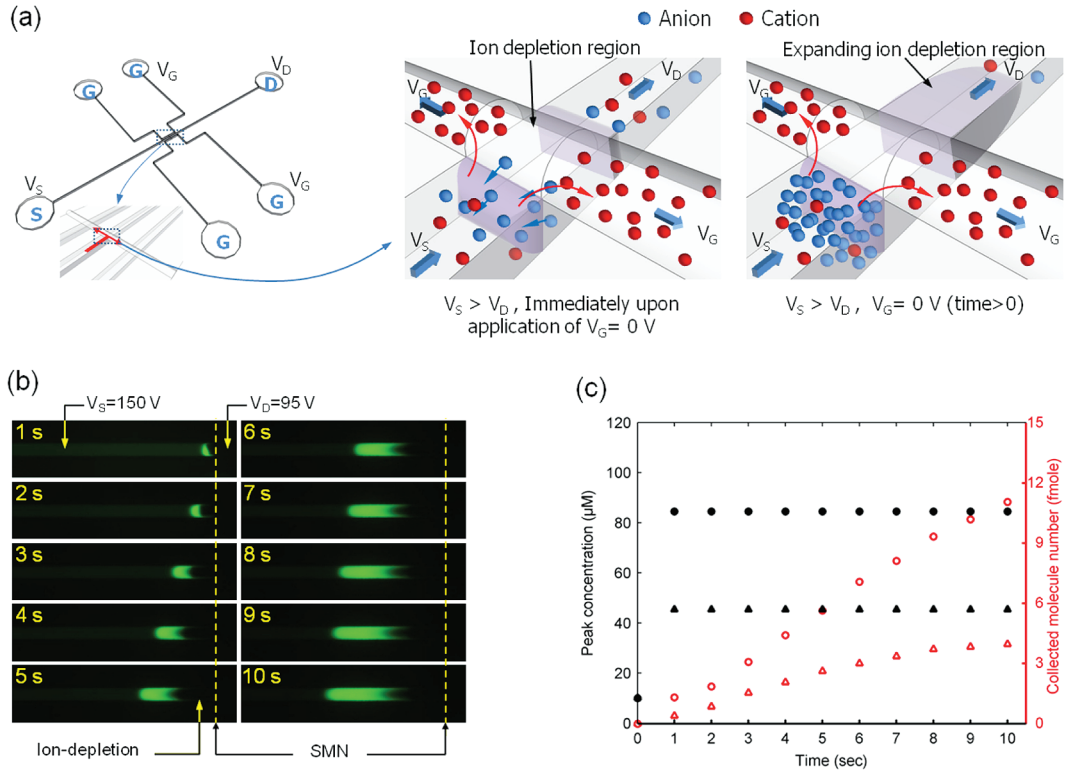

Figure 4. (a) Nano/micro ion preconcentrator (left) consists of a nanoslit engraved on a composite PDMS slab and microchannels in the glass substrate. The magnified schematics (right) explain the basic mechanism regulating the electrokinetic trapping process for ion preconcentration. The anions accumulate near the ion-depletion area where the EOF and EP find a balance. (b) Time-dependent formation of ion plugs near a nanoslit by applying a potential difference between the sample and ground channels. Fluorescence images were collected every 1 s over 10 s: the plug shapes remained stable after 10 s. As time passed, the fluorescence signal intensity and size increased due to the sample preconcentration. (c) Sample preconcentration results using a 10 μM fluorescein solution in phosphate buffer at pH 7.4. Peak concentration (black) and collected molecule number (femtomole) calculated from integrated fluorescence intensities over the entire preconcentrated plug (red) are shown at 100 (△,▲) and 200 (○,●) μM buffers, respectively.

permselectivity did not result from a reversible nanogap between the PDMS−glass bonding layer[43] but through the fabricated nanoslit.

CONCLUSIONS

In summary, we rapidly fabricated nanofluidic devices within a few hours (see the Supporting Information, Figure S4) via the surface tension-driven self-organization of a SU-8 mold. The width and height of the nanoslit mold were independently and easily tuned by regulating the contact time of the PDMS stamp and by changing the sliding speed of SU-8 and its viscosity, respectively. The use of composite layers of hard and soft PDMS, combined with the arch-shaped cross-section, allowed low aspect ratio (down to 0.02) nanoslit fabrication. Using the PDMS nanoslits, we successfully demonstrated the feasibility of our system as an ion preconcentrator via electrokinetic trapping in combination with electroosmotic and electrophoretic flow. The outstanding features of our proposed method are the rapid development of nanofluidic prototypes using only basic laboratory equipment and the precise control over nanoslit mold dimensions (height and width) using a simple one-step process.

ASSOCIATED CONTENT

Supporting Information. Microscope images of soft- and composite-PDMS nanoslit, time-dependent formation of ion plugs, time lapse for rapid prototyping of the nanoslit, and AFM image analysis of the SU-8 mold. This material is available free of charge via the Internet at http://pubs.acs.org.

AUTHOR INFORMATION

Corresponding Author

*E-mail: dbiomed@korea.ac.kr. Phone: +82-2-940-2881. Fax: +82-2-921-6818.

ACKNOWLEDGMENT

This research was supported by the Basic Science Research Program (Grant R11-2008-044-02002-0) and the Converging Research Center Program (Grant 2011K000677) through the National Research Foundation of Korea (NRF), funded by the Ministry of Education, Science and Technology. Chang-Beom Kim and Honggu Chun contributed equally to this work.

REFERENCES

(1) Baldessari, F.; Santiago, J. G. *J. Nanobiotechnol.* **2006**, *4*, 12–17.
(2) Stein, D.; Kruithof, M.; Dekker, C. *Phys. Rev. Lett.* **2004**, *93*, 035901.
(3) Pu, Q.; Yun, J.; Temkin, H.; Liu, S. *Nano Lett.* **2004**, *4*, 1099–1103.
(4) Sparreboom, W.; van den Berg, A.; Eijkel, J. C. T. *Nat. Nanotechnol.* **2009**, *4*, 713–720.

(5) Salieb-Beugelaar, G. B.; Teapal, J.; van Nieuwkasteele, J.; Wijnperle', D.; Tegenfeldt, J. O.; Lisdat, F.; van den Berg, A.; Eijkel, J. C. T. *Nano Lett.* **2008**, *8*, 1785–1790.
(6) Stein, D.; Deurvorst, Z.; van der Heyden, F. H. J.; Koopmans, W. J. A.; Gabel, A.; Dekker, C. *Nano Lett.* **2010**, *10*, 765–772.
(7) Wang, Y.; Han, J. *Lab Chip* **2008**, *8*, 392–394.
(8) Schmidt-Rohr, K.; Chen, Q. *Nat. Mater.* **2008**, *7*, 75–83.
(9) Liu, S.; Pu, Q.; Gao, L.; Korzeniewski, C.; Matzke, C. *Nano Lett.* **2005**, *5*, 1389–1393.
(10) Reccius, C. H.; Stavis, S. M.; Mannion, J. T.; Walker, L. P.; Craighead, H. G. *Biophys. J.* **2008**, *95*, 273–286.
(11) Mannion, J. T.; Reccius, C. H.; Cross, J. D.; Craighead, H. G. *Biophys. J.* **2006**, *90*, 4538–4545.
(12) Liang, X.; Morton, K. J.; Austin, R. H.; Chou, S. Y. *Nano Lett.* **2007**, *7*, 3774–3780.
(13) Cao, H.; Yu, Z.; Wang, J.; Tegenfeldt, J. O.; Austin, R. H.; Chen, E.; Wu, W.; Chou, S. Y. *Appl. Phys. Lett.* **2002**, *81*, 174–176.
(14) Park, J. Y.; Takayama, S.; Lee, S. -H. *Integr. Biol.* **2010**, *2*, 229–240.
(15) Whitesides, G. M. *Nature* **2006**, *442*, 368–373.
(16) Huh, D.; Mills, K. L.; Zhu, X.; Burns, M. A.; Thouless, M. D.; Takayama, S. *Nat. Mater.* **2007**, *6*, 424–428.
(17) Chung, S.; Lee, J. H.; Moon, M. -W.; Han, J.; Kamm, R. D. *Adv. Mater.* **2008**, *20*, 3011–3016.
(18) Park, S.; Huh, Y. S.; Craighead, H. G.; Erickson, D. *Proc. Natl. Acad. Sci. U.S.A.* **2009**, *106*, 15549–15554.
(19) Chun, H.; Chung, T. D.; Ramsey, J. M. *Anal. Chem.* **2010**, *82*, 6287–6292.
(20) Lee, J. H.; Song, Y. -A.; Tannenbaum, S. R.; Han, J. *Anal. Chem.* **2008**, *80*, 3198–3204.
(21) Kovarik, M. L.; Jacobson, S. C. *Anal. Chem.* **2007**, *79*, 1655–1660.
(22) Chung, S. H.; Choi, B. J.; Lee, S. W.; Yoon, D. S. *Biomed. Eng. Lett.* **2011**, *1*, 7–10.
(23) Kumar, A.; Biebuyck, H. A.; Whitesides, G. M. *Langmuir* **1994**, *10*, 1498–1511.
(24) Wilbur, J. L.; Kumar, A.; Kim, E.; Whitesides, G. M. *Adv. Mater.* **1994**, *6*, 600–604.
(25) Biebuyck, H. A.; Whitesides, G. M. *Langmuir* **1994**, *10*, 2790–2793.
(26) Odom, T. W.; Love, J. C.; Wolfe, D. B.; Paul, K. E.; Whitesides, G. M. *Langmuir* **2002**, *18*, 5314–5320.
(27) Odom, T. W.; Thalladi, V. R.; Love, J. C.; Whitesides, G. M. *J. Am. Chem. Soc.* **2002**, *124*, 12112–12113.
(28) Perry, J. M.; Zhou, K.; Harms, Z. D.; Jacobson, S. C. *ACS Nano* **2010**, *7*, 3897–3902.
(29) Xia, Y.; Whitesides, G. M. *J. Am. Chem. Soc.* **1995**, *117*, 3274–3275.
(30) Krausch, G. *Mater. Sci. Eng., R.* **1995**, *14*, 1–94.
(31) Korczagin, I.; Golze, S.; Hempenius, M. A.; Vancso, G. J. *Chem. Mater.* **2003**, *15*, 3663–3668.
(32) Sharpe, R. B. A.; Burdinski, D.; Huskens, J.; Zandvliet, H. J. W.; Reinhoudt, D. N.; Poelsema, B. *Langmuir* **2004**, *20*, 8646–8651.
(33) Kang, H.; Lee, J.; Park, J.; Lee, H. H. *Nanotechnology* **2006**, *17*, 197–200.
(34) Choi, K. M.; Rogers, J. A. *J. Am. Chem. Soc.* **2003**, *125*, 4060–4061.
(35) Schmid, H.; Michel, B. *Macromolecules* **2000**, *33*, 3042–3049.
(36) Hlushkou, D.; Dhopeshwarkar, R.; Crooks, R. M.; Tallarek, U. *Lab Chip* **2008**, *8*, 1153–1162.
(37) Zhou, K.; Kovarik, M. L.; Jacobson, S. C. *J. Am. Chem. Soc.* **2008**, *130*, 8614–8616.
(38) Kim, S. J.; Ko, S. H.; Kang, K. H.; Han, J. *Nat. Nanotechnol.* **2010**, *5*, 297–301.
(39) Lee, J. H.; Chung, S.; Kim, S. J.; Han, J. *Anal. Chem.* **2007**, *79*, 6868–6873.
(40) Wang, Y.; Stevens, A. L.; Han, J. *Anal. Chem.* **2005**, *77*, 4293–4299.
(41) Kim, P.; Kim, S. J.; Han, J.; Suh, K. Y. *Nano Lett.* **2010**, *10*, 16–23.
(42) Kim, H.; Kim, J.; Kim, E. -G.; Heinz, A. J.; Kwon, S.; Chun, H. *Biomicrofluidics* **2010**, *4*, 043014.
(43) Kim, S. M.; Burns, M. A.; Hasselbrink, E. F. *Anal. Chem.* **2006**, *78*, 4779–4785.